AIAA 96-2502

A Method for the Constrained Design of Natural Laminar Flow Airfoils

Bradford E. Green and John L. Whitesides
The George Washington University
Hampton, VA

Richard L. Campbell and Raymond E. Mineck
NASA Langley Research Center
Hampton, VA

14th AIAA Applied Aerodynamics Conference

June 17-20, 1996

New Orleans, LA

A METHOD FOR THE CONSTRAINED DESIGN OF NATURAL LAMINAR FLOW AIRFOILS

Bradford E. Green* and John L. Whitesides†
Joint Institute for Advancement of Flight Sciences
The George Washington University
NASA Langley Research Center
Hampton, VA

Richard L. Campbell‡ and Raymond E. Mineck§
Transonic/Supersonic Aerodynamics Branch
NASA Langley Research Center
Hampton, VA

Abstract

A fully automated iterative design method has been developed by which an airfoil with a substantial amount of natural laminar flow can be designed, while maintaining other aerodynamic and geometric constraints. Drag reductions have been realized using the design method over a range of Mach numbers, Reynolds numbers and airfoil thicknesses. The thrusts of the method are its ability to calculate a target N-Factor distribution that forces the flow to undergo transition at the desired location; the target-pressure-N-Factor relationship that is used to reduce the N-Factors in order to prolong transition; and its ability to design airfoils to meet lift, pitching moment, thickness and leading-edge radius constraints while also being able to meet the natural laminar flow constraint. The method uses several existing CFD codes and can design a new airfoil in only a few days using a Silicon Graphics IRIS workstation.

Nomenclature

A	relaxation factor for N-Factor design method
C_p	pressure coefficient
c_l	section lift coefficient
c_m	pitching moment coefficient
N	N-Factor
s	chordwise distance from the leading-edge
x	non-dimensional distance along chord of airfoil

Greek

λ	relaxation factor used to meet lift constraint
ς	relaxation factor used to meet pitching moment constraint

Subscript

a	analysis
cp	control point
des	design
j	airfoil station
$stag$	stagnation point
T	target
tol	tolerance
u	upper surface

Superscript

i	iteration index

Introduction

For many years, reducing drag has been a major issue in airplane design. Reductions in drag allow airplanes to operate more efficiently by using less fuel, which results in reduced operating costs and smaller, quieter engines. The design of airplanes with bigger payloads and longer ranges is also possible when drag is reduced.

There have been many attempts to reduce airplane drag. Since the 1930's, there has been a great interest in designing airfoils and wings for natural laminar flow (NLF) to reduce viscous drag. In addition, supercritical wings were developed to reduce the wave drag on airplanes. The use of winglets on airplanes today also demonstrates an attempt to reduce airplane drag. This

---

* Graduate Research Scholar Assistant, AIAA Student Member
† Professor of Engineering and Applied Science, Associate Fellow of AIAA
‡ Research Engineer, Senior Member of AIAA
§ Research Engineer

paper presents a design method for reducing drag through the design of NLF airfoils.

This new design method[1] combines proven CFD analysis and design codes with a new target pressure design technique. A flowchart of the method is shown in figure 1. Starting from an initial airfoil, the flow solver, which is an Euler solver[2,3,4] coupled with a turbulent boundary layer method[5], is used to calculate the pressure distribution of the starting airfoil. Then, a laminar boundary layer solver[6] is used to calculate the boundary layer velocity and temperature profiles. These profiles are then used by COSAL[7], the stability analysis code, to calculate the N-Factors of the current airfoil. Using the current pressures and N-Factors, the Target Pressure Design module then calculates a target pressure distribution that increases the amount of laminar flow over the airfoil.

Once the target pressures are known, the CDISC airfoil design method[8] then iteratively designs a new airfoil which possesses this target pressure distribution. The target pressures for the design are then modified in the Modify Target Pressures to Enforce Constraints module while using the airfoil design method such that the aerodynamic constraints are achieved[1]. After designing a new airfoil, the boundary layer profiles are then calculated once again by the laminar boundary layer solver so that the stability analysis code can calculate the N-Factors of the new airfoil. If all of the design constraints are met, then the method terminates. Otherwise, the method will continue to iterate until the prescribed number of iterations is achieved.

The Target Pressure Distribution

After choosing an initial airfoil, the pressure distribution of the airfoil is calculated using the Euler solver, and the N-Factor envelope of the airfoil is calculated using the laminar boundary layer solver and the stability analysis code. Then, from the current pressure and N-Factor distributions, a target pressure distribution is calculated that meets all of the aerodynamic constraints. The module labeled Target Pressure Design in figure 1 is responsible for calculating this new target pressure distribution. Figure 2 shows a detailed flowchart of how the Target Pressure Design module calculates the new target pressures. Each of the components in this flowchart will now be discussed.

The Target N-Factor Distribution

Once the analysis N-Factor distribution has been calculated by the stability analysis code, a target N-Factor distribution must be prescribed, as demonstrated by the first module in figure 2. This target N-Factor distribution must force the flow to undergo transition at the desired location.

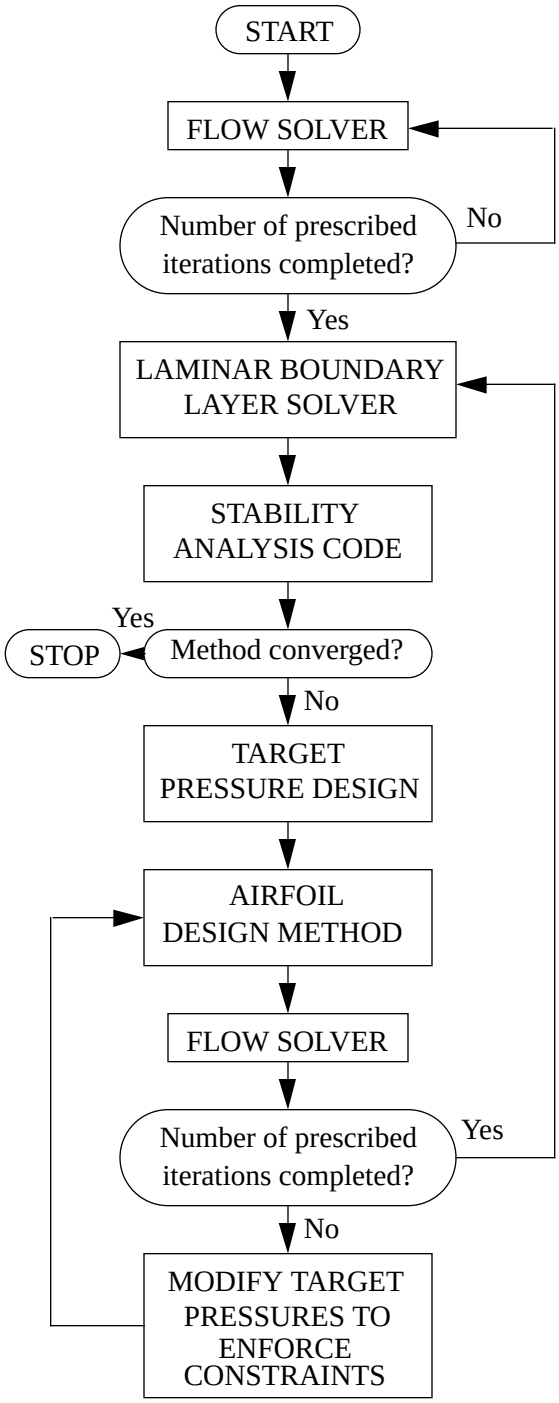

Figure 1. A flowchart of the NLF airfoil design method

In order to calculate the target N-Factor distribution, four control points ($x_{cp,1}$, $x_{cp,2}$, $x_{cp,3}$ and $x_{cp,4}$) are specified. The first control point is located at the point where the analysis N-Factors first become greater than an N-Factor level, $N_{cp,1}$. Ahead of the first control point, the analysis N-Factors are kept as the

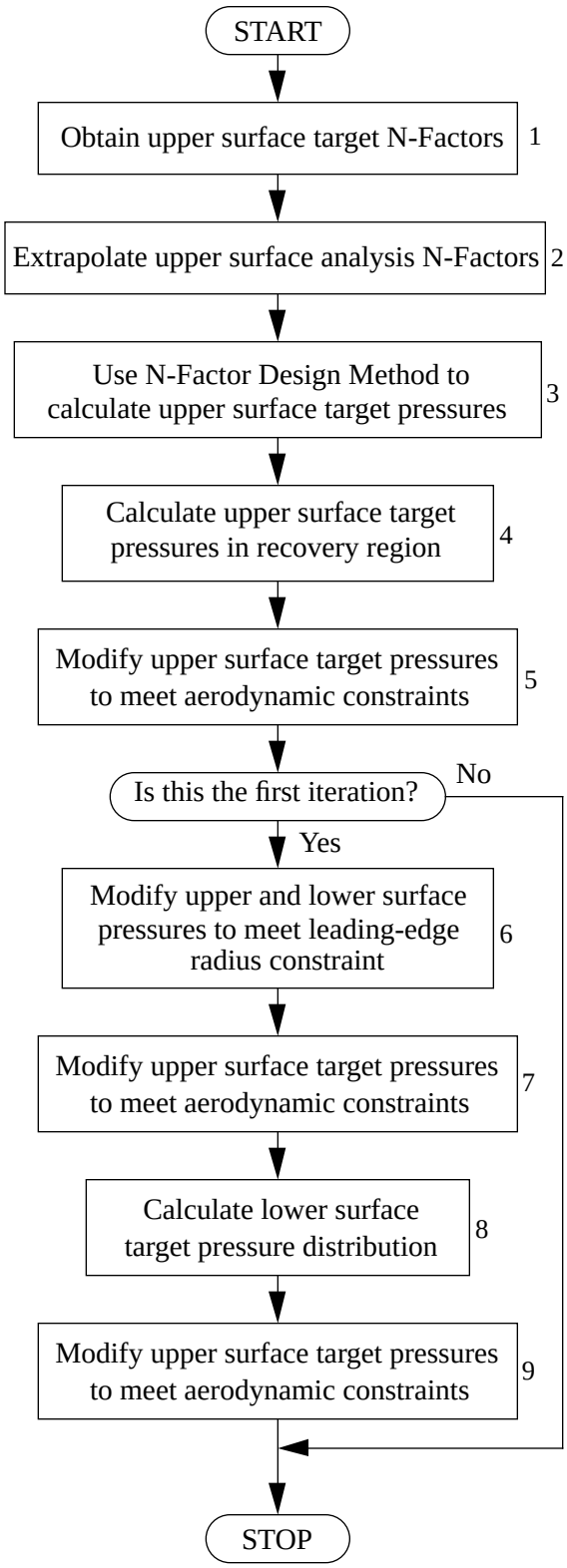

Figure 2. A flowchart of the Target Pressure Design module

target N-Factors. Beyond this point, the other control points and their N-Factor levels are used to calculate the target N-Factors. This is done by connecting each consecutive control point with a straight line, then smoothing the curve using a polynomial fit.

Figure 3 shows a typical target N-Factor distribution and the control points used to calculate these target N-Factors. In this figure, $x_{cp,2} = 0.58$, $x_{cp,3} = 0.60$, $x_{cp,4} = 0.65$, $N_{cp,1} = 3$, $N_{cp,2} = 8$, $N_{cp,3} = 10$, and $N_{cp,4} = 15$. Ahead of $x_{cp,2}$, the target N-Factor distribution forms a buffer region above which the N-Factors aren't allowed to grow so that the flow will not undergo transition at slightly off-design conditions. Then, between $x_{cp,2}$ and $x_{cp,4}$, the N-Factors are allowed to grow rapidly to force transition at 60% chord for this case.

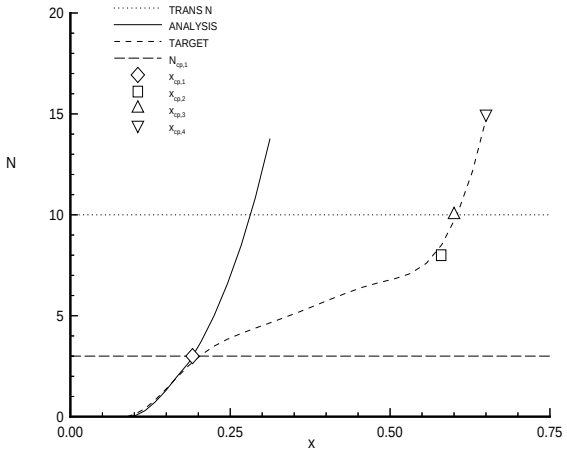

Figure 3. A typical target N-Factor distribution with control points

Moreover, the third control point is placed at the location of desired transition, and a nominal transition N-Factor of 10 is used. Actually, the transition N-Factor could have been as low as eight or as high as 15. For this purpose, the N-Factors were allowed to grow rapidly between the second and fourth control points. This reduces the uncertainty in the transition location by increasing the N-Factor gradient in the transition region.

Extrapolation of Analysis N-Factors

The stability analysis code can calculate N-Factors only when the boundary layer is attached. This causes problems if the boundary layer of the current airfoil separates ahead of the fourth control point, $x_{cp,4}$. The second module in figure 2 is included to remedy this situation.

Suppose the boundary layer of the current airfoil separates at airfoil station k, say at 30% chord. In addition, suppose that the fourth control point is located at airfoil station l, say at 65% chord. This indicates that analysis N-Factors exist only to 30% chord, while the target N-Factors have been specified back to 65% chord. In the N-Factor design method, which will be discussed in the next section, both analysis and target N-Factors must be known ahead of the fourth control point.

For this reason, a method was developed to extrapolate the analysis N-Factors from station k to station l. The method extrapolates the N-Factors based on the pressures between the two stations. At any station j between k and l, the analysis N-Factors are calculated as

$$N_j = N_{j-1} + \frac{N_{j-1} - N_{j-2}}{C_{p,\,a,\,j-1,\,u} - C_{p,\,a,\,j-2,\,u}} \times \times \left(C_{p,\,a,\,j,\,u} - C_{p,\,a,\,j-1,\,u}\right) \tag{1}$$

where $C_{p,\,a,\,j,\,u}$ represents the upper surface analysis pressure coefficient at station j.

The N-Factor Design Method

After calculating the target N-Factor distribution and extrapolating the analysis N-Factors, the N-Factor design method calculates a target pressure distribution that moves the analysis N-Factors toward the target N-Factors. This method, which is shown as the third module in the flowchart in figure 2, is based on a target pressure-N-Factor relationship that was developed. In this method, the change in pressure coefficient required at airfoil station j to move the analysis N-Factor at j, N_j, toward the target N-Factor at j, $N_{T,\,j}$, is

$$\frac{\Delta C_{p,\,j}}{\Delta x_j} = A \Delta N_j \tag{2}$$

where

$$\Delta C_{p,\,j} = C_{p,\,T,\,j,\,u} - C_{p,\,a,\,j,\,u} \tag{3}$$

$$\Delta x_j = \left| x_j - x_{j-1} \right| \tag{4}$$

$$\Delta N_j = N_{T,\,j} - N_j \tag{5}$$

In these equations, A is a relaxation parameter (typically 0.50), $C_{p,\,T,\,j,\,u}$ is the upper surface target pressure at station j, $C_{p,\,a,\,j,\,u}$ is the upper surface analysis pressure at station j, and Δx_j is the grid spacing.

In order to maintain a smooth and continuous target pressure distribution, once $\Delta C_{p,\,j}$ has been calculated at station j, this change in C_p is applied to all of the stations downstream of j as well. In doing this, the flow downstream of j has been changed and, as a result, it is necessary to correct the analysis N-Factors downstream. This is done by adding ΔN_j to each of the analysis N-Factors aft of j. Equation 2 can then be rewritten to account for the corrections made downstream. The target pressure coefficient that results at an airfoil station j is

$$C_{p,\,T,\,j,\,u} = \left(C_{p,\,a,\,j,\,u} + \Delta C_{p,\,j-1,\,u}\right) + + A \Delta x_j \left(N_{T,\,j} - \left(N_j + \Delta N_{j-1}\right)\right) \tag{6}$$

With $j = 1$ corresponding to the stagnation point, this relation is valid from $j = 2$ to $j = l$, where l is the airfoil station representing the fourth control point, $x_{cp,\,4}$. The boundary conditions at the stagnation point are

$$C_{p,\,T,\,1,\,u} = C_{p,\,a,\,1,\,u} = C_{p,\,stag} \tag{7}$$

$$N_{T,\,1} = N_1 = 0 \tag{8}$$

This method is used only to design the upper surface target pressures since the lower surface target pressures are only modified to meet the geometric constraints.

The Pressures in the Recovery Region

Once the target pressures have been calculated ahead of station l, the target pressures in the recovery region are calculated, as demonstrated by the fourth module on the flowchart in figure 2. These target pressures are determined based on the analysis pressures in the recovery region of the initial airfoil that was analyzed and a linear pressure coefficient distribution that is eventually used to modify the pressure distribution to meet the pitching moment constraint.

In order to calculate the target pressures in this region, two intermediate pressure distributions are determined. The first intermediate pressure distribution, $C_{p,\,j,\,1}$, is determined by linearly scaling the pressures of the initial airfoil, $C_{p,\,j,\,0}$. (The linear scaling method used is described in Appendix A of reference 1.) As a result, the first intermediate pressure distribution is calculated using the relation

$$C_{p,\,j,\,1} = C_{p,\,n,\,0} + + \frac{C_{p,\,T,\,l,\,u} - C_{p,\,n,\,0}}{C_{p,\,l,\,0} - C_{p,\,n,\,0}} \left(C_{p,\,j,\,0} - C_{p,\,n,\,0}\right) \tag{9}$$

where n is the trailing-edge station. This expression is valid from $j = l$ to $j = n$.

The second intermediate pressure distribution, $C_{p,\,j,\,2}$, is determined by adding a linear pressure coefficient distribution to $C_{p,\,j,\,0}$. As a result,

$$C_{p,\,j,\,2} = C_{p,\,j,\,0} + \frac{1 - x_j}{0.30} C_{p,\,0.7c} \tag{10}$$

where $C_{p,\,0.7c}$ is the magnitude of the linear pressure coefficient distribution at 70% chord. This equation is also valid from $j = l$ to $j = n$.

Finally, the target pressures in the recovery region are calculated by taking a weighted average of the first and second intermediate pressure recoveries. (The weighted averaging technique is discussed in Appendix B of reference 1.) The upper surface target pressures in the recovery region then become

$$C_{p,\,T,\,j,\,u} = \frac{x_n - x_j}{x_n - x_l} C_{p,\,j,\,1} + \frac{x_j - x_l}{x_n - x_l} C_{p,\,j,\,2} \qquad (11)$$

Equation 11 is used from $j = l$ to $j = n$.

Meeting the Aerodynamic Constraints

The upper surface target pressures that have been calculated must now be modified to meet the lift and pitching moment constraints. This is shown in the fifth module on the flowchart shown in figure 2.

In order to modify the target pressure distribution to meet the aerodynamic constraints, the upper surface target pressure distribution is divided into three distinct regions. The leading-edge region extends from the leading-edge of the airfoil to the last station where the N-Factors are zero, which is represented by station m. The center region extends from station $m + 1$ to l, the location of the fourth control point. This is the region where the N-Factors are growing most rapidly. Finally, the recovery region extends from station $l + 1$ to n, the trailing-edge.

A method was developed to modify the target pressures in such a way that the upper surface NLF would not be disturbed while meeting the aerodynamic constraints. A detailed flowchart of this process is shown in figure 4. Once c_l and c_m have been calculated, the lift constraint is checked. If $|c_{l,\,des} - c_l| > c_{l,\,tol}$, then $\Delta C_{p,\,c}$ is calculated and the target pressures in the three regions are modified. With

$$\Delta C_{p,\,c} = \frac{2\lambda s_n (c_{l,\,des} - c_l)}{s_l - s_m + s_n} \qquad (12)$$

the new target pressures in the center and leading-edge regions are, respectively,

$$C^{i+1}_{p,\,T,\,j,\,u} = C^{i}_{p,\,T,\,j,\,u} + \Delta C_{p,\,c} \qquad (13)$$

$$C^{i}_{p,\,T,\,j,\,u} = C^{i}_{p,\,T,\,1,\,u} + \frac{C^{i+1}_{p,\,T,\,m,\,u} - C^{i}_{p,\,T,\,1,\,u}}{C^{i}_{p,\,T,\,m,\,u} - C^{i}_{p,\,T,\,1,\,u}} \left(C^{i}_{p,\,T,\,j,\,u} - C^{i}_{p,\,T,\,1,\,u} \right) \qquad (14)$$

where i denotes the old target pressures, $i + 1$ denotes the new target pressures, λ is a relaxation factor (typically 0.50) and

$$s_j = \sum_{k=2}^{j} |x_k - x_{k-1}| \qquad (15)$$

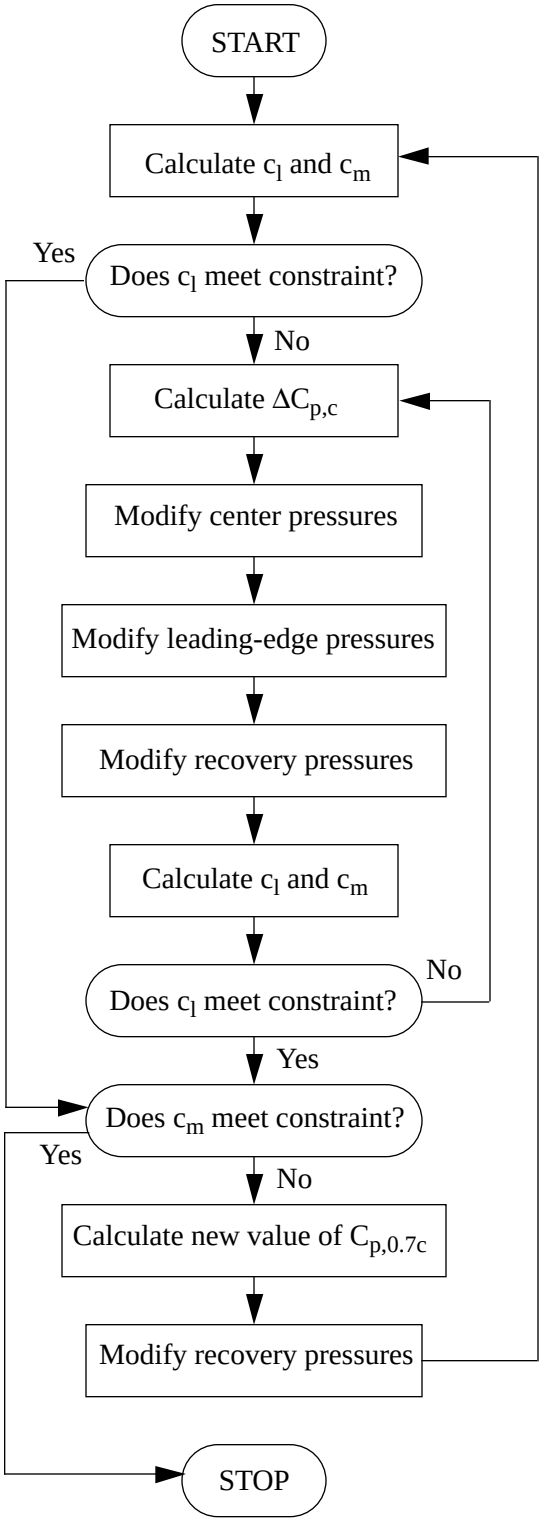

Figure 4. A flowchart of how the upper surface target pressures are modified to meet the aerodynamic constraints

Once the target pressures in the leading-edge and center regions have been calculated, the method of the previous section is used to calculate the new target pressures in the recovery region. As shown in the flowchart in figure 4, this process is iterated until $|c_{l,des} - c_l| \le c_{l,tol}$.

Once the lift coefficient meets the desired tolerance $c_{l,tol}$ (typically 0.01), a new value of $C_{p,0.7c}$ is calculated to modify the target pressures to meet the pitching moment constraint. The new value of $C_{p,0.7c}$ is calculated as

$$C_{p,0.7c}^{i+1} = C_{p,0.7c}^{i} + \frac{24\varsigma\,(c_{m,des} - c_m)}{(1-x_l)\,(8x_l + 1)} \qquad (16)$$

where i denotes the old value of $C_{p,0.7c}$ and ς is a relaxation factor (typically 0.50). Once the new value of $C_{p,0.7c}$ has been calculated, the method of the previous section is used once again to calculate the target pressures in the recovery region. The target pressures are then modified again to meet the lift constraint. This method is iterated until $|c_{l,des} - c_l| \le c_{l,tol}$ and $|c_{m,des} - c_m| \le c_{m,tol}$, where $c_{m,tol}$ is the pitching moment tolerance (typically 0.01). The development of this entire method can be found in reference 1.

Once the upper surface target pressures have been modified to meet the aerodynamic constraints, the upper and lower surface target pressures are modified to meet the leading-edge radius constraints. Then, after modifying the upper surface target pressures to once again meet the aerodynamic constraints, the lower surface target pressures are calculated. These lower surface target pressures are determined by linearly scaling the upper surface target pressures. Once this is done, the upper surface target pressures are once again modified to meet the aerodynamic constraints. The processes of modifying the target pressures to meet the leading-edge radius constraint and calculating the lower surface target pressures will not be discussed here. They have been discussed in detail in reference 1.

Results

The NLF airfoil design method that has been described in the previous sections will now be used to design several airfoils for a variety of flow conditions and constraints.

Airfoil for a General Aviation Application

The first airfoil that is presented was designed for the same flow conditions and constraints for which the NLF(1)-0414F airfoil[9,10] was designed. The NLF(1)-0414F has already been tested in a wind-tunnel. This airfoil was designed to have 70% chord NLF on both surfaces at a Mach number of 0.40, a Reynolds number of 10 million and a lift coefficient of 0.40. In order to have NLF to 70% chord, the N-Factor at 70% chord was to be less than nine on both surfaces. In addition, the airfoil was to be 14% thick and have a trailing-edge cruise flap with the pressures in the recovery region being determined using an energy method. When the boundary layer had the most energy, the pressure gradient was to be the most adverse. Then, as the boundary layer loses energy, the pressure gradient was to become less adverse so that turbulent separation would be avoided at the design condition.

The NLF(1)-0414F was designed iteratively using the NYU code[11,12,13] to calculate the pressures of each intermediate airfoil and the SALLY code[14] to perform the stability analysis. Modifications were then made by hand to the airfoil geometry to give the airfoil the desired characteristics.

Starting with the NACA 64_1-212 airfoil, a new airfoil was designed by the NLF airfoil design method that would meet the same constraints as the NLF(1)-0414F. Since the NLF airfoil design method does not have the capability to use an energy method to prescribe the pressures in the recovery region, the pitching moment coefficient was constrained by the NLF airfoil design method to be -0.08 on the new airfoil. In addition, the airfoil thickness at 85%, 90% and 95% chord were constrained by the NLF airfoil design method to prevent the trailing-edge from being too thin.

Figure 5 shows a comparison of the new airfoil and the NLF(1)-0414F. The airfoils designed by the two different techniques appear to be very similar. Since the leading-edge radius was not constrained in either design, there is a slight difference between the two airfoils in the leading-edge region which is reflected in the mid-chord region. If the leading-edge radius had been constrained, perhaps the airfoils would be even more similar.

Figure 6 shows a comparison of the pressure distributions of the two airfoils. In general, these pressure distributions also appear to be very similar. There is a little difference in the leading-edge pressures due to the difference in the leading-edge radius of the two airfoils. The pressures in the mid-chord region compare very well although they are slightly off-set. This may be due to the fact that the NLF airfoil design method was able to maintain the thickness of the new airfoil to be exactly 14% chord, while the maximum thickness of the NLF(1)-0414F is actually 14.3% chord. The bumps in the pressure distribution on the lower surface of the new airfoil in the recovery region are due to the thickness constraints imposed at 85%, 90% and 95% chord.

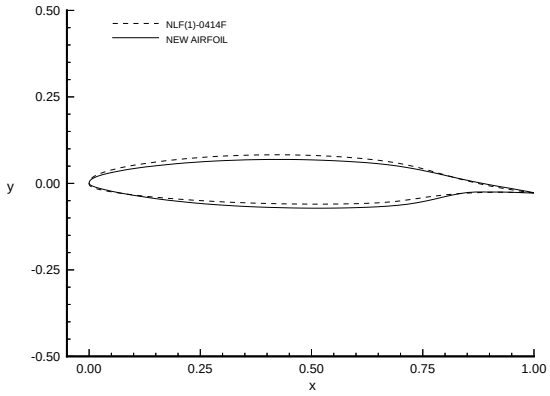

Figure 5. A comparison of the NLF(1)-0414F and the new airfoil

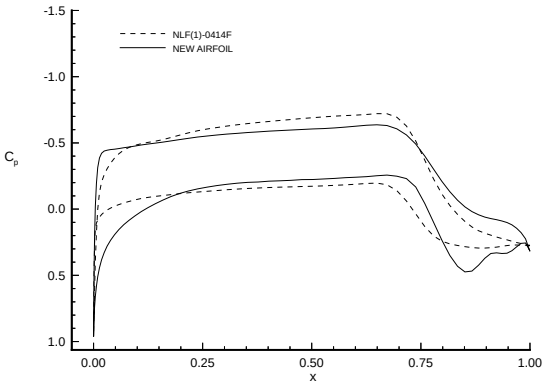

Figure 6. A comparison of the pressures of the NLF(1)-0414F and the new airfoil at M = 0.40, Re = 10 million, and $c_l = 0.40$

Figure 7 shows a comparison of the upper and lower surface N-Factor distributions of the two airfoils. The N-Factors at 70% chord on the new airfoil are less than nine, as was prescribed. The target N-Factor distribution discussed previously (see figure 3) was not used in this design since that type of distribution was not prescribed in the design of the NLF(1)-0414F. In figure 7, the N-Factor distributions of the new airfoil possess the same general shape as the N-Factor distributions of the NLF(1)-0414F. In order to meet the lower surface N-Factor constraint, the lower surface of the airfoil was designed by inverting the airfoil and designing it at $-c_{l,\,des}$ and $-c_{m,\,des}$. This was done since the N-Factor design method discussed previously can only prescribe the target pressures on the upper surface of the airfoil so that the N-Factor constraint is achieved.

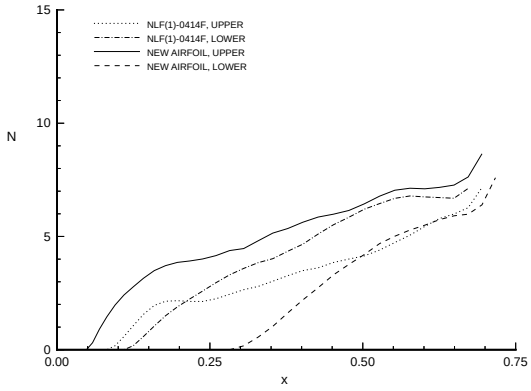

Figure 7. A comparison of the N-Factor distributions of the NLF(1)-0414F and the new airfoil at M = 0.40, Re = 10 million, and $c_l = 0.40$

The design of the NLF(1)-0414F airfoil took approximately one year, while the design of the new airfoil using the NLF airfoil design method took only two days on a Silicon Graphics Indigo2 workstation with an R4000 processor.

Airfoil for a Glider Application

As the second application of the NLF airfoil design method, the glider airfoil presented in reference 1 will be redesigned to improve the laminar flow characteristics of the lower surface. The glider airfoil was designed for 65% chord upper surface NLF at a Mach number of 0.10, a Reynolds number of 3 million, a lift coefficient of 0.30, and a pitching-moment coefficient of -0.06. In addition, the airfoil was to be 15% thick with a leading-edge radius of 1.4% chord. Front and rear spar constraints were also enforced.

In redesigning this airfoil, 65% chord NLF is desired on both surfaces while maintaining the lift and pitching moment constraints, and the maximum thickness and leading-edge radius constraints. It was assumed that the front and rear spar thicknesses could not be constrained while maintaining the desired amount of NLF on the lower surface. As a result, the front and rear spar constraints were removed for the current design.

Figure 8 shows a comparison of the glider airfoil from reference 1 and the redesigned airfoil. The redesigned airfoil meets the maximum thickness constraint of 15% chord and has a leading-edge radius of 1.38% chord. Notice that the redesigned airfoil is thicker than the glider airfoil in the region from 50% to 80% chord. This increase in thickness was the

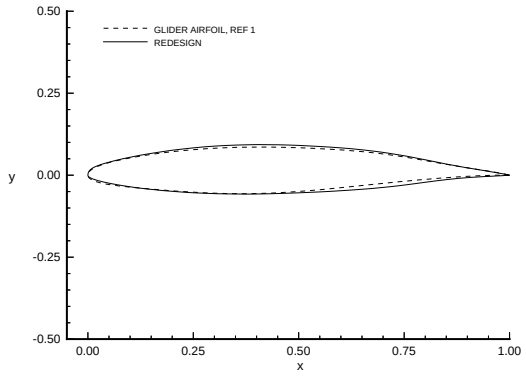

Figure 8. A comparison of the glider airfoil from reference 1 and the redesigned airfoil

mechanism by which a more favorable pressure gradient was imposed on the lower surface so that laminar flow could be increased. This can be seen in figure 9, which compares the pressure distributions of the two airfoils.

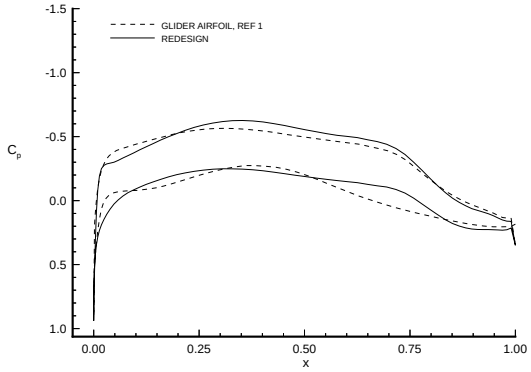

Figure 9. A comparison of the pressure distributions of the glider airfoil from reference 1 and the redesigned airfoil at M = 0.10, Re = 3 million, and c_l = 0.30

Figure 10 shows a comparison between the upper and lower surface N-Factor distributions of the redesigned airfoil and the target N-Factor distributions. In this plot, a nominal N-Factor of 13.5 was used to estimate the location of transition. On both surfaces, the N-Factor distributions meet the target N-Factor distributions. As a result, NLF was achieved on both surfaces to 65% chord. The plot also shows the lower surface N-Factor distribution for the glider airfoil of reference 1. The upper surface N-Factor distribution of the glider airfoil is not shown in this plot since it did not change much during the design.

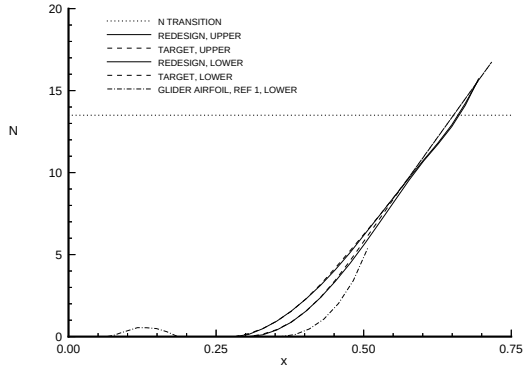

Figure 10. The upper and lower surface N-Factor distributions of the redesigned airfoil at M = 0.10, Re = 3 million, and c_l = 0.30

Airfoil for a Commuter Aircraft

As the final example, the commuter airfoil in reference 1 was redesigned to increase the amount of NLF on the lower surface, since a laminar flow constraint was only implemented on the upper surface in the design of this airfoil. This airfoil was designed at a Mach number of 0.60, a Reynolds number of 20 million and a lift coefficient of 0.40. The airfoil was to be 12% thick, with a leading-edge radius of 1% chord. In the current design, it was desired to maintain 60% chord NLF on both surfaces with a pitching moment coefficient of -0.08.

In the current design, repeated attempts were made to design a 12% thick airfoil with a 1% chord leading-edge radius, while meeting the NLF and aerodynamic constraints. In these attempts, the upper and lower NLF constraints were not being achieved while maintaining both the thickness and leading-edge radius constraints. As a result, the leading-edge radius constraint was released so that both of the NLF constraints could be achieved. Maintaining the leading-edge radius constraint would have required the maximum thickness of the airfoil to be larger than 12% chord. While maintaining the maximum thickness constraint, the leading-edge radius of the redesigned airfoil was 0.78% chord. All of the other constraints were achieved in this design.

Figure 11 shows the redesigned airfoil and its pressure distribution at the design conditions. The favorable pressure gradients to 70% chord on both surfaces are responsible for the flow remaining laminar. Figure 12 shows the upper and lower surface N-Factor distributions of the airfoil at the design conditions. In this figure, an N-Factor of 10 was used to

estimate the location of transition. This critical value was varied from the previous example to show that the NLF airfoil design method works for various transition N-Factors. In this plot, the N-Factor distributions meet the target N-Factor distributions that were imposed in order to force the flow to undergo transition at 60% chord.

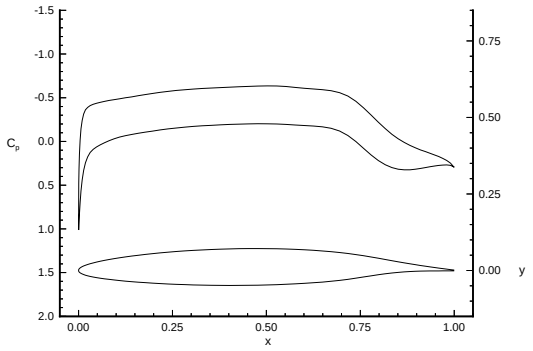

Figure 11. The redesigned commuter airfoil and its pressure distribution at M = 0.60, Re = 20 million, and c_l = 0.40

The upper surface target N-Factor distribution in this plot resembles the target N-Factor distribution that was discussed previously (see figure 3). The target N-Factor distribution in figure 12 forms a buffer region ahead of 50% chord where the N-Factors are not allowed to grow above eight. Then, from 50% to 70% chord, the N-Factors are allowed to grow rapidly to force the flow to transition at 60% chord.

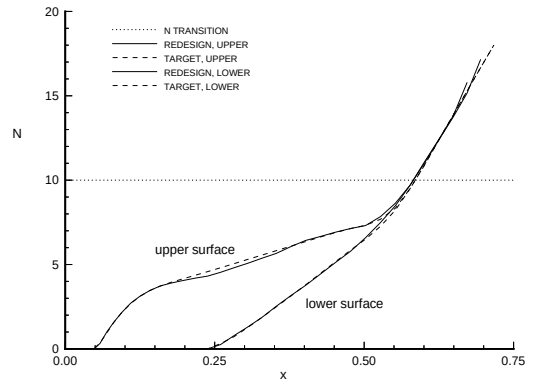

Figure 12. The upper and lower surface N-Factor distributions of the redesigned commuter airfoil at M = 0.60, Re = 20 million, and c_l = 0.40

Concluding Remarks

An automated two-dimensional method has been developed for designing NLF airfoils, while maintaining several other aerodynamic and geometric constraints. The method has been shown to work for a range of Mach numbers, Reynolds numbers, and airfoil thicknesses.

In order to develop this NLF airfoil design method, several existing CFD codes were coupled together. In addition, a process was developed for calculating a target N-Factor distribution that forces transition to occur at the desired location. Using this target N-Factor distribution, as well as the current analysis N-Factors and pressures, a method was also developed for calculating a target pressure distribution. Using this target pressure distribution, the current airfoil is redesigned to obtain a new airfoil that is closer to meeting the desired NLF, aerodynamic and geometric constraints. This method has been used to design a number of airfoils, with results shown for glider, general aviation and commuter applications.

There are several possibilities for extension of this research. The method could be applied to bodies other than airfoils and wings, with possible applications including fuselages and nacelles. In addition, the method could be extended to the design of airfoils for supersonic applications. Since large sweep angles are needed for supersonic wings, crossflow instabilities would be a major issue. In these cases, boundary layer suction and blowing is often necessary to help reduce the crossflow disturbances. As a result, when extending the method to include supersonic designs, the method may also have to be modified to account for suction and blowing.

Acknowledgments

This research was conducted in partial fulfillment of a Master of Science degree with the George Washington University and was completed at NASA Langley Research Center.

References

1. Green, B.E.: “An Approach to the Constrained Design of Natural Laminar Flow Airfoils,” Master’s Thesis, The George Washington University, 1995.

2. Hartwich, P.M.: “Comparison of Coordinate-Invariant and Coordinate-Aligned Upwinding for the Euler Equations,” *AIAA Journal*, Vol. 32, No. 9, September 1994, pp. 1791-1799.

3. Hartwich, P.M.: “Euler Study on Porous Transonic Airfoils with a View Toward Multipoint Design,” *Jour-*

nal of Aircraft, Vol. 30, No. 2, March-April 1993, pp. 184-191.

4. Hartwich, P.M.: "Fresh Look at Floating Shock Fitting," *AIAA Journal*, Vol. 29, No. 7, July 1991, pp. 1084-1091.

5. Stratford, B.S.; and Beavers, G.S.: "The Calculation of the Compressible Turbulent Boundary Layer in an Arbitrary Pressure Gradient - A Correlation of Certain Previous Methods," R. & M. No. 3207, British Aeronaut. Res. Coun., September 1959.

6. Iyer, V.: "Computation of Three-Dimensional Compressible Boundary Layers to Fourth-Order Accuracy on Wings and Fuselages," NASA CR-4269, January 1990.

7. Malik, M.R.: "COSAL - A Black-Box Compressible Stability Analysis Code for Transition Prediction in Three-Dimensional Boundary Layers," NASA CR-165925, May 1982.

8. Campbell, R.L.: "An Approach to Constrained Aerodynamic Design with Application to Airfoils," NASA TP-3260, November 1992.

9. Viken, J.K.: "Aerodynamic Design Considerations and Theoretical Results for a High Reynolds Number Laminar Flow Airfoil," Master's Thesis, The George Washington University, 1983.

10. McGhee, R.J.; Viken, J.K; Pfenninger, W.; Beasley, W.D.; and Harvey, W.D.: "Experimental Results for a Flapped Natural-Laminar-Flow Airfoil with High Lift/ Drag Ratio," NASA TM-85788, May 1984.

11. Bauer, F.; Garabedian, P.; and Korn, D.: "A Theory of Supercritical Wing Sections, with Computer Programs and Examples," New York: Springer-Verlag, 1972.

12. Bauer, F.; Garabedian, P.; and Korn, D.; and Jameson, A.: "Supercritical Wing Sections II," New York: Springer-Verlag, 1975.

13. Bauer, F.; Garabedian, P.; and Korn, D.: "Supercritical Wing Sections III," New York: Springer-Verlag, 1977.

14. Srokowski, A.J.; and Orszag, S.A.: "Mass Flow Requirements for LFC Wing Design," AIAA Paper 77-1222, 1977.